Microsc. Microanal. 8, 422–428, 2002
DOI: 10.1017/S1431927602010309

Microscopy AND Microanalysis

Measuring Thickness Changes in Thin Films Due to Chemical Reaction by Monitoring the Surface Roughness with *In Situ* Atomic Force Microscopy

L.Y. Beaulieu,[1] A.D. Rutenberg,[1] and J.R. Dahn[1,2]*

[1]*Physics Department, Dalhousie University, Halifax, NS B3H 3J5, Canada*
[2]*Chemistry Department, Dalhousie University, Halifax, NS B3H 3J5, Canada*

Abstract: Measuring the changing thickness of a thin film, without a reference, using an atomic force microscope (AFM) is problematic. Here, we report a method for measuring film thickness based on *in situ* monitoring of surface roughness of films as their thickness changes. For example, *in situ* AFM roughness measurements have been performed on alloy film electrodes on rigid substrates as they react with lithium electrochemically. The addition (or removal) of lithium to (or from) the alloy causes the latter to expand (or contract) reversibly in the direction perpendicular to the substrate and, in principle, the change in the overall height of these materials is directly proportional to the change in roughness. If the substrate on which the film is deposited is not perfectly smooth, a correction to the direct proportionality is needed and this is also discussed.

Key words: alloy film electrodes, atomic force microscope, expansion and contraction, Li-ion battery, surface roughness, thin film thickness, volume changes

Introduction

Since its inception, the atomic force microscope (AFM) has quickly become an invaluable tool in many branches of science. The reason for this success is due to the AFM's great versatility. Today's commercial AFM can be used for such tasks as surface imaging (from 100 μm to atomic resolution), phase detection, friction measurement, force sensing, and many more (Manne et al., 1991; Quate, 1994). Here, we will show how an AFM can be used *in situ* to infer film thickness changes due to chemical reaction from changes in surface roughness. No fixed reference is necessary.

Received May 23, 2001; accepted October 15, 2001.
**Corresponding author*. E-mail: jeff.dahn@dal.ca

The *in situ* AFM study of thickness changes in nickel hydroxide electrodes has been reported in Häring and Kötz (1995) and Kowal et al. (1996). In both these previous studies, the change in thickness of the electrode was studied by single point scanning. This method consists of maintaining the AFM tip of the nanoprobe at a constant point on the electrode while monitoring the elongation and contraction of the piezo necessary to maintain a constant force of the cantilever on the sample. Also, in both these cases, the height changes were observed over a span of only a few minutes. Although this method can be used to obtain changes in thickness it has two disadvantages. In the first case, single point scanning does not allow for the morphology of the surface to be studied while the thickness changes are occurring. This potentially presents a huge loss of information on

the mechanical properties of the sample. Secondly, due to the high temperature sensitivity of most SPMs, it is very difficult to measure the thickness changes of a sample for long periods of time. A change of one degree can easily induce sample drift, which can cause uncertainties in the measurements described above. In this article, we propose a new method for monitoring thickness changes *in situ* by AFM while obtaining the sample topography information at the same time.

To improve the storage capabilities of portable batteries, a large amount of research has been redirected from alkaline batteries to the study of lithium-ion batteries. Recently metallic alloys M (M = Si, Sn, Al, etc.) have been proposed as possible negative electrode materials for lithium-ion batteries (Yang et al., 1996; Idota et al., 1997; Mao et al., 1999; Beaulieu et al., 2000). These alloys can undergo expansions by up to 300% when they react with lithium to their composition limit, Li_xM, where x can be as large as 4.4 for M = Si or Sn. Thin films of suitable alloys can be prepared by sputtering on metallic substrates and such films can be directly used as electrodes in test electrochemical cells. In an effort to learn about the volume changes and fracturing of these films caused by the reactions with lithium, we recently constructed a facility for *in situ* atomic force microscopy of these alloy electrodes directly in electrochemical cells (Beaulieu et al., 2001a, 2001b). These studies showed how the surface roughness of the films changed in a reversible manner correlated with the lithium content and presumably the film thickness. Here, we report and analyze the roughness variations of these alloy films as they react with lithium.

Experimental

The AFM system used has already been described in Beaulieu et al. (2001a). Briefly, a Molecular Imaging (Phoenix, AZ) PicoScan SPM with a 37-μm AFM scanner was placed in a Vacuum Atmospheres (Hawthorne, CA) double glove box with water and oxygen levels below 1 ppm. Imaging was performed using constant force contact mode with sharpened Si_3N_4 nanoprobes (Digital Instruments). All electrochemical reactions were conducted in a shop-made, open-face, two-electrode wet cell with lithium serving as both the counter and reference electrode. The electrolyte used was 1 M $LiPF_6$ dissolved in a 50:50 volume mixture of ethylene carbonate and propylene carbonate. Samples (Turner, 2000) were prepared by sputtering $Si_{0.7}Sn_{0.3}$ ($\sim$1.2 μm thick) films on Cu (4 μm thick) coated metal (400 series stainless steel, 1 cm diameter, 2 mm thick) substrates. The substrates were previously polished to a mirror-like finish with an RMS roughness of about 10 nm as measured by the AFM. The sputtered deposits were amorphous by X-ray diffraction. The electrochemical reaction of lithium with the samples was performed using constant current with a computer-controlled Keithley 236 source/measure unit.

Results

Figure 1 shows the results of an *in situ* experiment performed on a typical film over a time period of 100 hr. AFM topographic images were acquired continuously throughout. Figure 1j at the bottom shows the voltage versus both time (bottom abscissa) and scan number (top abscissa) for the electrodecycled versus pure lithium metal. The voltage curve is described as a series of nine discharge/charge cycles. During the discharge cycle, lithium is added to the alloy, and during the charge cycle, lithium is removed from the alloy. Figure 1a–i shows a small selection of AFM images collected during this experiment. Figure 1a is 19 $\times$ 19 μm and Figures 1b–i are 37 $\times$ 37 μm. The location of Figure 1a is shown in Figure 1c by a white frame. When lithium is added to the alloy film for the first time, the film expands in the direction perpendicular to the substrate. Measurements performed by *in situ* optical microscopy show no lateral change in the film dimension during this first discharge cycle (Beaulieu et al., 2001b).

During the first charge cycle (removing lithium from the alloy), the film contracts almost uniformly in all directions, causing the film to crack in a manner analogous to the desiccation of wet mud (Groisman and Kaplan, 1994; Kitsunezaki, 1999). The crack pattern formed during this first charge cycle is maintained throughout the duration of the subsequent cycles. As lithium is further added and removed, the particles expand and contract while remaining attached to the substrate at the center of the particle. Figure 1b–f show the electrode as lithium is inserted (Fig. 1b–d) and then removed (Fig. 1e,f). Inserting lithium into the electrode causes the film to expand as described above. The expansion of the film causes the cracks to close (Fig. 1c,d). Removing the lithium causes the cracks to reopen once again. As more lithium is added and removed from the electrode, the effects become more pronounced.

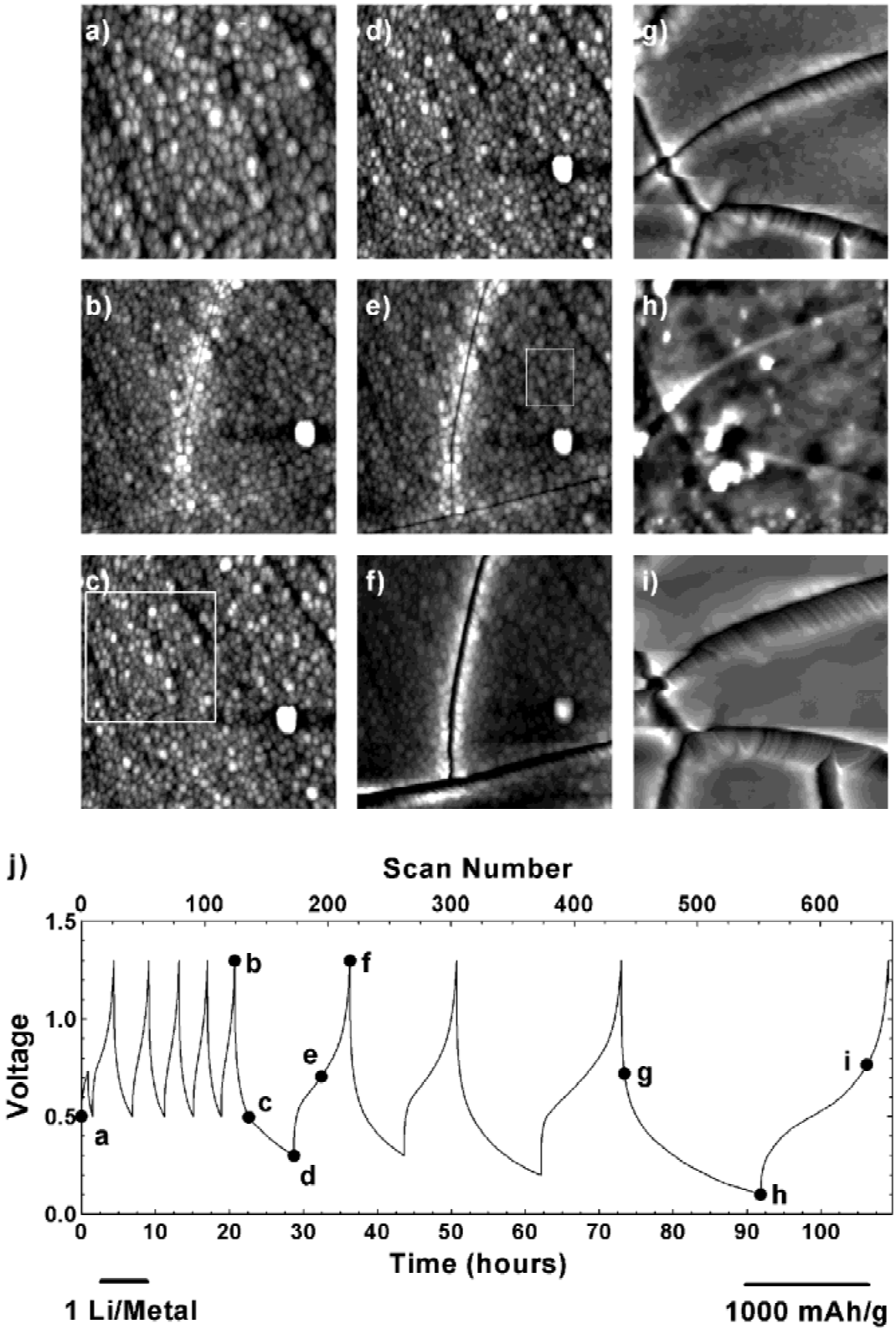

Figure 1. *In situ* AFM experiment performed on a Si-Sn electrode. The AFM image (**a**) is 19 × 19 μm and the AFM images (**b** to **i**) are 37 × 37 μm in size. The contrast scale from dark to light corresponds to (**a**) 0 to 160 nm, (**b**) 0 to 165 nm, (**c**) 0 to 160 nm, (**d**) 0 to 170 nm, (**e**) 0 to 210 nm, (**f**) 0 to 400 nm, (**g**) 0 to 1000 nm, (**h**) 0 to 280 nm, and (**i**) 0 to 2000 nm. **j**: The voltage versus time (bottom abscissa) and AFM scan number (top abscissa). The bars in the lower part of **j** show the time corresponding to 1 Li/metal and 1000 mAh/g at the current used.

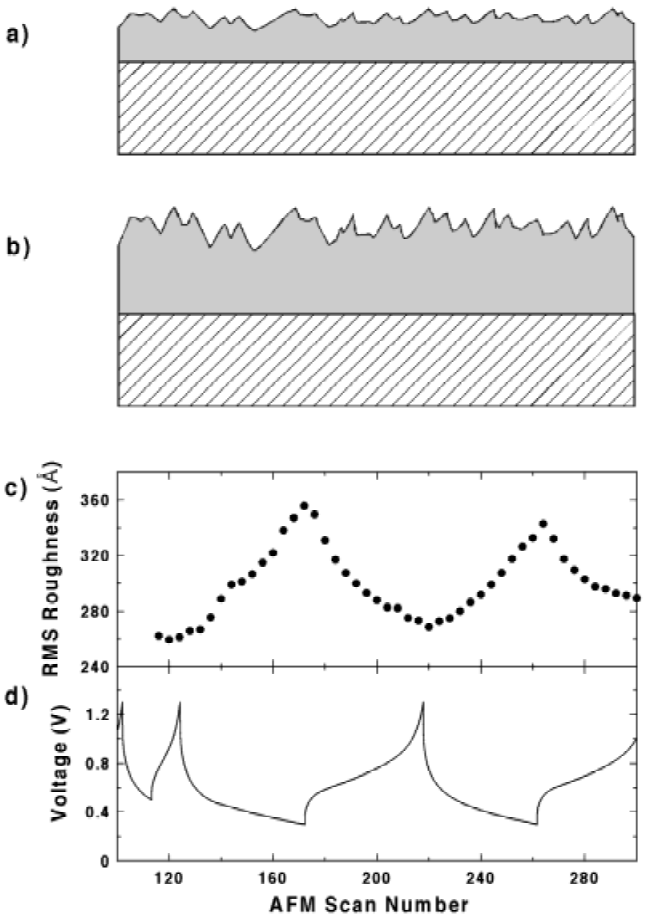

Figure 2. (**a**) Schematic representation of a rough film on a smooth substrate. (**b**) Schematic representation of the film in (**a**) that has doubled in thickness. (**c**) Change in RMS roughness of the electrode surface compared to (**d**), the voltage versus AFM scan number.

Figure 1g, taken at a different location on the electrode surface, shows how the cracks become larger as lithium is removed from the film. Reinserting lithium into the films shows how the expansion causes the film to buckle up against itself at the cracked edges (Fig. 1h). Figure 1i shows once again how the cracks expand further still as lithium is removed from the electrode.

It is difficult to obtain a sense of the changes in film thickness from the images presented in Figure 1. In fact, Figures 1c and 1d look almost identical to the eye. It is only when one performs a statistical analysis that one learns Figure 1d (RMS roughness = 33.5 nm) is much rougher than 1c (RMS roughness = 26.9 nm). This suggests that the film has expanded vertically in a perfectly proportional manner. Panels a and b of Figure 2 schematically show that if the thickness of a thin film on a smooth substrate increases everywhere, so does the roughness. To study the changes in roughness of the film, it is very important that the area analyzed remain well adhered to the substrate. It is also important that the area chosen be the same for all measurements. Therefore the region shown by the white square in Figure 1e was chosen for the statistical analysis.

From the images collected for the experiment shown above, the RMS roughness (standard deviation) was calculated as a function of lithium content. As is customary, the RMS roughness was defined as:

$$R_{RMS} = \sqrt{\frac{\sum_{i=1}^{N} (z_i - \bar{z})^2}{N}}, \tag{1}$$

where N is the total number of data points, z_i is the vertical coordinate of the image, and $\bar{z}$ is the mean value of the z_is. The bottom panels in Figure 2 show the RMS roughness (Fig. 2c) of the highlighted area in Figure 1e compared to the voltage curve collected during the experiment (Fig. 2d). The RMS roughness is a function of the lithium content in the electrode. As lithium is added to the electrode (scan numbers 124 to 172 and 217 to 262) the roughness increases. Similarly, as the lithium is removed from the electrode (scan numbers 172 to 217 and 262 to 304) the roughness decreases.

Equation (1) shows that if all points of the film double (for example) in height, then so does the RMS roughness. Hence, from the fractional change in roughness, one could then deduce the total growth of the film. This analysis, however, assumes that the underlying substrate is perfectly smooth.

The average roughness of a thin film sample is a convolution of the roughness of the substrate and of the film. To illustrate this point, consider a hypothetical film with surface height $z(x, y)$ of average thickness t with an inherent roughness $\Delta z(x, y)$, deposited on an initially rough substrate with height $s(x, y)$. With these definitions, $z(x, y) = s(x, y) + t + \Delta z(x, y)$. Assume that a Gaussian distribution $P(s)$ can describe the surface roughness of the substrate. In the same way, a Gaussian distribution $P(\Delta z)$ can be used to describe the inherent roughness of the film. These distributions are written as follows:

$$P(s) = Ae^{-(s)^2/2\sigma_s^2} \tag{2}$$

$$P(\Delta z) = Be^{-(\Delta z)^2/2\sigma_{\Delta z}^2}, \tag{3}$$

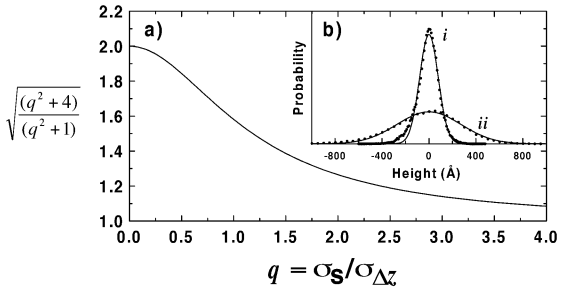

Figure 3. (**a**) RMS roughness of lithiated film $\sigma_{lf} = \sqrt{(q^2+4)/(q^2+1)}$ plotted as a function of $q = \sigma_s/\sigma_{\Delta z}$, showing the effect of substrate roughness on the ability to measure the doubling of film thickness. (**b**) Panel *i*: height distribution of stainless steel substrate. Panel *ii*: height distribution of the Si-Sn film.

where A and B are normalization factors, and σ_s and $\sigma_{\Delta z}$ are the standard deviations of the substrate height and the film thickness, respectively. To obtain the standard deviation of the film surface, we take the convolution of the substrate height and the film thickness as follows:

$$P(z) = AB \iint e^{-(s)^2/2\sigma_s^2} e^{-(\Delta z)^2/2\sigma_{\Delta z}^2} \times \delta(z - (s + t + \Delta z))\, d\Delta z\, ds \tag{4}$$

$$= AB \int e^{-(s)^2/2\sigma_s^2} e^{-(z-s-t)^2/2\sigma_{\Delta z}^2}\, ds \tag{5}$$

$$= Ce^{-(z-t)^2/2(\sigma_s^2+\sigma_{\Delta z}^2)}. \tag{6}$$

From equation (6) we obtain the RMS roughness (standard deviation) of the film height: $\sigma_z = \sqrt{\sigma_s^2 + \sigma_{\Delta z}^2}$. This equation shows how the roughness of the substrate influences the roughness measurements of the film surface. Doing the same analysis for a film which expands α times its initial height ($t \to \alpha t$ and $\Delta z(x, y) \to \alpha \Delta z(x, y)$), we get an RMS roughness, σ_{lf} (*lf*: lithiated film), equal to $\sigma_{lf} = \sqrt{\sigma_s^2 + (\alpha\sigma_{\Delta z})^2}$. Taking the ratio σ_{lf}/σ_z, we get a function of the form $\sqrt{(q^2+\alpha^2)/(q^2+1)}$, where $q = \sigma_s/\sigma_{\Delta z}$. This function, plotted in Figure 3 for $\alpha = 2$, shows the effects of the rough substrate. Since $\sigma_{\Delta z}$ is fixed, increasing the roughness of the substrate quickly prevents direct determination of the change in film height from the change in surface roughness. Figure 3b shows the distribution of the surface heights for both the substrate (i) and film surface (ii). The circles represent the data and the straight lines represent the Gaussian fits. As can be seen, excellent agreement is obtained.

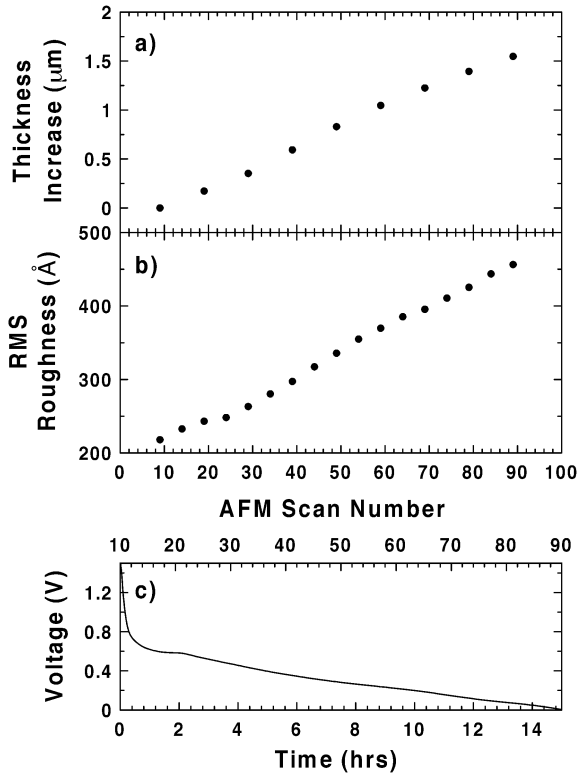

Figure 4. Change in height of the electrode occurring during the first discharge measured using (**a**) the raw data, and (**b**) the change in surface RMS roughness compared to (**c**) the voltage curve collected during the experiment.

Figure 4 shows the results of an *in situ* AFM experiment conducted on a similar Si-Sn electrode as shown in Figure 1. Figure 4c shows the voltage versus both time (bottom abscissa) and AFM scan number (top abscissa) collected during the first complete discharge (insertion of lithium into the electrode) of this cell. During the discharge, the AFM topographic images were collected continuously. To minimize effects due to thermal drift, the system was maintained at 30°C using a Watlow (Winona, MN) heating element and controller. Figure 4a shows the change in height calculated from the unflattened raw data collected during this experiment. Each image was fitted to a plane and then the average distance between the first image (scan number 9) and each subsequent image was calculated. This analysis gives a film growth of 1.5 ± 0.2 μm, which, when added to the original film thickness of 1.2 ± 0.1 μm, gives an overall film thickness of 2.7 ± 0.2 μm at the bottom of discharge. Figure 4b shows the results of monitoring the RMS roughness of the AFM images collected during the discharge. As mentioned in the Experimental section, pol-

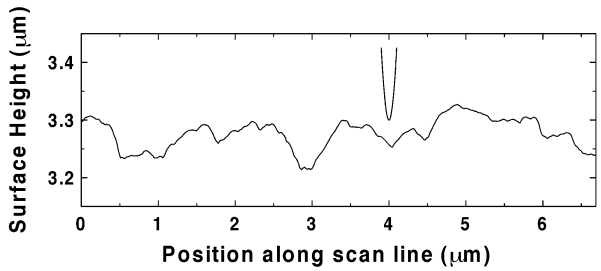

Figure 5. AFM cross section compared to an AFM tip described by a parabola with a 40-nm radius apex.

ished stainless steel substrates were sputter coated with Cu and SiSn in succession. Because we could not get a direct measurement of the RMS roughness of the Cu layer, we used the value of $\sigma_S = 10 \pm 0.1$ nm found from averaging the RMS roughness of the stainless steel substrate measured from several samples. Hence, using the analysis presented above gives a value of $\alpha = 2.1 \pm 0.2$ using $q = 0.5 \pm 0.6$. Applying this value to the initial thickness gives an overall thickness of 2.6 ± 0.2 μm, which agrees well with the results obtained from monitoring the piezo in the scanner.

The advantage of using the roughness measurements to extrapolate the thickness changes over that of monitoring the contraction and/or elongation of the piezo ceramic in the scanner is that roughness changes are independent (up to a limit) of thermal changes. For example, the geometry of our system is such that the sample is held beneath the scanner by three stainless steel supports approximately 1 cm in length. A one-degree change in temperature can cause linear expansion in these supports of over 100 nm. This elongation is then transmitted directly to the piezo as it tries to maintain a constant force of the cantilever on the sample (in the case where constant force contact mode is being used) and is registered as a spurious sample growth. However, as long as the sample is still within reach of the scanner, the roughness measurements are completely unaffected by changes in temperature.

For the sake of completeness, tip effects on our roughness measurements have also been considered. All AFM images are a convolution of the actual surface of the sample and the shape of the cantilever tip. It can easily be shown that for samples with small surface features, the measured roughness is much smaller than the actual surface roughness (Dongmo et al., 1998). Figure 5 shows a typical cross section of an AFM image of one of our SiSn films and a sketch of the tip, to scale. The size of the predominant surface features is in the micrometer range, whereas the radius of the tip is in the 40-nm range. It is clear that the finite radius of the tip is not influencing the measurements.

Conclusions

We have shown, using a simple experiment and analysis, that AFM roughness measurements can be used to infer film thickness changes in cases where the film thickness changes proportionally at all points of the film. However, the roughness of the substrate on which the film is initially deposited is an important factor to be considered, for it influences the experimental results profoundly. When quantitative results are needed, the use of smooth or previously well-characterized substrates is recommended.

Acknowledgments

We thank the Natural Science and Engineering Research Council of Canada and 3M Canada Inc. for financial support of this work under the Industrial Research Chair and Research Grant programs. LYB also thanks NSERC and 3M Canada for a postgraduate scholarship.

References

Beaulieu, L.Y., Cumyn, V.K., Eberman, K.W., Krause, L.J. & Dahn, J.R. (2001a). A system for performing simultaneous *in situ* atomic force microscopy/optical microscopy on electrode materials for lithium-ion batteries. *Rev Sci Instrum* **72**, 3313–3319.

Beaulieu, L.Y., Eberman, K.W., Turner, R.L., Krause L.J. & Dahn, J.R. (2001b). Colossal reversible volume changes in lithium alloys. *Electrochem Solid St* **4**, A137–A140.

Beaulieu, L.Y., Larcher, D., Dunlap, R.A. & Dahn, J.R. (2000). Reaction of Li with grain-boundary atoms in nanostructured compounds. *J Electrochem Soc* **147**, 3206–3212.

Dongmo, S., Vautrot, P., Bonnet, N. & Troyon, M. (1998). Correction of surface roughness measurements in SPM images. *Appl Phys A* **66**, S819–S823.

Groisman, A. & Kaplan, E. (1994). An experimental-study of cracking induced by desiccation. *Europhys Lett* **25**, 415–420.

Häring, P. & Kötz, R. (1995). Nanoscale thickness changes of nickel-hydroxide films during electrochemical oxidation-reduction monitored by *in situ* atomic-force microscopy. *J Electroanal Chem* **385**, 273–277.

Idota, Y., Matsufuji, A., Maekawa, Y. & Miyasaka, T. (1997).

Tin-based amorphous oxide: A high-capacity lithium-ion-storage material. *Science* **276**, 1395–1397.

Kitsunezaki, S.O. (1999). Fracture patterns induced by desiccation in a thin layer. *Phys Rev E* **60**, 6449–6464.

Kowal, A., Niewiara, R., Peroczyk, B. & Haber, J. (1996). *In situ* atomic force microscopy observation of change in thickness of nickel hydroxide layer on Ni electrode. *Langmuir* **12**, 2332–2333.

Manne, S., Hansma, P.K., Massie, J., Elings, V.B. & Gewirth, A. (1991). Atomic-resolution electrochemistry with the atomic force microscope—Copper deposition on gold. *Science* **251**, 183–186.

Mao, O.U., Dunlap, R.A. & Dahn, J.R. (1999). Mechanically alloyed Sn-Fe-(C) powders as anode materials for Li-ion batteries—I. The Sn_2Fe-C system. *J Electrochem Soc* **146**, 405–413.

Quate, C.F. (1994). The AFM as a tool for imaging. *Surf Sci* **299**, 980–995.

Turner, R.L. (2000). World Intellectual Property Organization Patent Application WO 00/03444.

Yang, J., Winter, M. & Besenhard, J.O. (1996). Small particle size multiphase Li-alloy anodes for lithium-ion batteries. *Solid State Ionics* **90**, 281–290.